Published in final edited form as:

Cancer Immunol Res. 2020 March ; 8(3): 345–355. doi:10.1158/2326-6066.CIR-19-0517.

Combined CD44- and CD25-targeted Near-Infrared Photoimmunotherapy Selectively Kills Cancer and Regulatory T cells in Syngeneic Mouse Cancer Models

Yasuhiro Maruoka[1], **Aki Furusawa**[1], **Ryuhei Okada**[1], **Fuyuki Inagaki**[1], **Daiki Fujimura**[1], **Hiroaki Wakiyama**[1], **Takuya Kato**[1], **Tadanobu Nagaya**[1], **Peter L. Choyke**[1], **Hisataka Kobayashi**[1]

[1]Molecular Imaging Program, Center for Cancer Research, National Cancer Institute, NIH, Bethesda, MD, 20892, USA

Abstract

Near-infrared photoimmunotherapy (NIR-PIT) is a newly developed and selective cancer treatment that induces necrotic and immunogenic cell death and utilizes a monoclonal antibody conjugated to a photo-absorber dye, IR700DX, activated by NIR light. Although CD44 is surface cancer marker associated with drug resistance, anti-CD44-IR700 NIR-PIT results in inhibited cell growth and prolonged survival in multiple tumor types. Meanwhile, anti-CD25-IR700–targeted NIR-PIT has been reported to achieve selective and local depletion of $FOXP3^+CD25^+CD4^+$ regulatory T cells (Tregs), which are primary immunosuppressive cells in the tumor microenvironment (TME), resulting in activation of local antitumor immunity. Combined NIR-PIT with CD44- and CD25-targeted agents has the potential to directly eliminate tumor cells and also amplify the immune response by removing $FOXP3^+CD25^+CD4^+$ Tregs from the TME. We investigated the difference in therapeutic effects of CD44-targeted NIR-PIT alone, CD25-targeted NIR-PIT alone, and the combination of CD44- and CD25-targeted NIR-PIT in several syngeneic tumor models, including MC38-luc, LL/2, and MOC1. The combined NIR-PIT showed significant tumor growth inhibition and prolonged survival compared with CD44-targeted NIR-PIT alone in all tumor models and showed prolonged survival compared with CD25-targeted NIR-PIT alone in MC38-luc and LL/2 tumors. Combined CD44/CD25 NIR-PIT also resulted in some complete remissions, whereas this was not achieved with either type of NIR-PIT alone. Therefore, combined NIR-PIT simultaneously targeting cancer antigens and immunosuppressive cells in the TME may be more effective than either type of NIR-PIT alone and may have potential to induce prolonged immune responses in treated tumors.

Keywords

near-infrared photoimmunotherapy; monoclonal antibodies; CD44; CD25; regulatory T cell

Corresponding author: Hisataka Kobayashi, M.D., Ph.D., Molecular Imaging Program, Center for Cancer Research, National Cancer Institute, NIH, 10 Center Drive, Bethesda, MD, 20892, USA, Tel: 301-435-4086; Fax: 301-402-3191; kobayash@mail.nih.gov.

Disclosure of Potential Conflicts of Interest

The authors have no conflict of interest to disclose.

Introduction

Near-infrared photoimmunotherapy (NIR-PIT) is a newly developed cancer treatment that induces selective cell death in targeted tumor cells. It employs a monoclonal antibody (mAb) conjugated to a photo-absorber, silica-phthalocyanine (IRDye700DX: IR700) dye. The conjugate is intravenously injected, allowed to accumulate within the target cells, and then is selectively activated by NIR light application [1]. This antibody–photo-absorber conjugate is commonly directed at an antigen expressed on the cell membrane of tumor cells, and after exposure to NIR light, cell death is observed within minutes. NIR-PIT induces rapid necrotic and immunogenic cell death in targeted tumor cells, with minimal or no cytotoxic effects in adjacent normal cells [1–3]. Treated tumor cells exhibit rapid volume expansion, blebbing, cell membrane rupture, and extrusion of cell contents into the extracellular space [4], leading to an immunogenic cell death [5]. Phase I/II clinical studies of NIR-PIT in patients with inoperable head and neck cancer using a cetuximab (anti-EGFR)-IR700 conjugate have been completed, and a Phase III study is underway. (https://clinicaltrials.gov/ct2/show/NCT02422979).

CD44 is a well-known marker of cancer stem cells and is implicated in intercellular adhesion, cell migration, cell spatial orientation, and promotion of matrix-derived survival signals [6–8]. Cell transformation, uncontrolled cell growth, resistance to apoptosis, and active cell migration are mediated by CD44 along with other factors [9]. High expression of CD44 on the plasma membrane of tumors is associated with tumor aggressiveness, drug resistance, and poor outcome [10–12]. CD44 inhibition can impair tumor growth [7,10], and NIR-PIT using anti-CD44-IR700 can produce effective therapeutic responses in CD44-expressing syngeneic mouse models [13,14].

$FOXP3^+CD25^+CD4^+$ suppressive regulatory T cells (Tregs) are crucial for immunological self-tolerance to maintain immune homeostasis and prevent autoimmune disease [15,16]. They are widely regarded as one of the primary mediators of antitumor immunity suppression [17]. Tregs induce immunosuppression using a variety of mechanisms, including inhibiting IL10 and transforming growth factor-beta (TGFβ), suppression of natural killer (NK) cells and effector T cells through secretion of cytotoxic substances, suppression by metabolic disruption of effector T cells due to consumption of IL2, and suppression by modulation of dendritic cell (DC) maturation or function [18]. In several types of cancers, it has been reported that decreased ratios of $CD8^+$ T cells to $FOXP3^+CD25^+CD4^+$ Tregs in tumor-infiltrating lymphocytes (TILs) is associated with poor prognosis [19]. Although a variety of methods for systemic Treg depletion have been previously attempted [20–22], CD25-targeted NIR-PIT has been demonstrated to selectively deplete tumor-infiltrating Tregs within the tumor without eliminating local effector cells or Tregs in other organs, resulting in reversal of the permissive tumor microenvironment (TME) and subsequent tumor killing [23]. Thus, CD25-targeted NIR-PIT has great potential to enhance tumor-directed NIR-PIT in that it can eliminate immunosuppressive cells in the TME.

NIR-PIT can simultaneously target two or more kinds of cells by co-injecting two or more different antibody–photo-absorber conjugates, followed by exposure to NIR light

[24,25]. CD44 is expressed on the cell membrane in various types of cancers [9] and $FOXP3^+CD25^+CD4^+$ Tregs are also frequently found within tumors [26]. Therefore, we hypothesized that combining anti-CD44– and anti-CD25–targeted NIR-PIT could achieve greater therapeutic benefits compared to NIR-PIT based on either target alone. The purpose of this study was to compare the *in vivo* therapeutic efficacy of NIR-PIT using CD44-targeted NIR-PIT alone, CD25-targeted NIR-PIT alone, and the combination of both CD44- and CD25-targted NIR-PIT in syngeneic mouse models of cancer.

Materials and Methods

Cell culture

MC38 cells (colon cancer, kind gift from Claudia Palena, NCI, 2015) stably expressing luciferase (MC38-luc, generated via stable transduction with RediFect Red-Fluc lentivirus from PerkinElmer per manufacturer recommendations), LL/2 cells (Lewis lung carcinoma; kind gift of James Hodge, NCI, 2015), and MOC1 cells (murine oral carcinoma, kind gift from Ravindra Uppaluri, Washington University in St. Louis, 2014) were used in this study. High luciferase expression on the MC38-luc cells was confirmed through 10 passages. MC38-luc and LL/2 cells were cultured in RPMI 1640 supplemented with 10% fetal bovine serumand 1% penicillin-streptomycin (all Gibco brand, Thermo Fisher Scientific) in tissue culture flasks (182 cm^2, CELLTREAT Scientific Products) in a humidified incubator at 37°C in an atmosphere of 95% air and 5% carbon dioxide. MOC1 cells were cultured in HyClone Iscove's Modified Dulbecco's Medium (IMDM; GE Healthcare Life Sciences)/ HyClone Ham's Nutrient Mixture F12 (GE Healthcare Life sciences) at a 2:1 mixture with 5% fetal bovine serum, 1% penicillin/streptomycin, 5 ng/mL epidermal growth factor (EGF; EMD Millipore Corporation), 400 ng/mL hydrocortisone (Sigma-Aldrich), and 5 mg/mL insulin (Sigma-Aldrich) in the tissue culture flasks in a humidified incubator at 37°C in an atmosphere of 95% air and 5% carbon dioxide. Cell line are routinely tested to be Mycoplasma-negative using MycoAlert PLUS Mycoplasma Detection Kit (Lonza) and cultured no more than for 30 passages. Cells were authenticated via *in vitro* growth characteristics

Reagents

Water soluble, silica-phthalocyanine derivative, IRDye700DX NHS ester was obtained from LI-COR Bioscience (Lincoln, NE, USA). An anti-mouse/human CD44 (IM7) and anti-mouse CD25 (PC-61.5.3) were purchased from Bio X Cell. All other chemicals were of reagent grade.

Synthesis of IR700-conjugated anti-CD44 and anti-CD25

Briefly, anti-CD44–IgG (1 mg, 6.7 nmol/L) and anti-CD25 (1 mg, 6.7 nmol/L) were respectively incubated with IR700 (65.1 μg, 33.3 nmol, 10 mmol/L in DMSO) and 0.1 mol/L Na_2HPO_4 (pH 8.5) at room temperature for 1 hour. The mixture was purified with a gel filtration column (Sephadex G 25 column, PD-10, GE Healthcare, Piscataway, NJ, USA). The protein concentration was determined with Coomassie Plus protein assay kit (Thermo Fisher Scientific Inc, Rockford, IL, USA) by measurement of the absorption at 595 nm with spectroscopy (8453 Value System; Agilent Technologies, Santa Clara, CA,

USA). We abbreviated IR700-conjugated anti-CD44 and anti-CD25 as anti-CD44-IR700 and anti-CD25-IR700, respectively.

Animal model

All procedures were performed in compliance with the Guide for the Care and Use of Laboratory Animals and approved by the local Animal Care and Use Committee. Six- to eight-week-old female C57BL/6 mice (strain #000664) were purchased from the Jackson laboratory. The lower part of the body of the mice was shaved before NIR light irradiation and image analysis. MC38-luc cells (8 million), LL/2 cells (8 million), and MOC1 cells (4 million) were subcutaneously injected in the dorsum of the mice. Mice with tumors reaching approximately 150 mm^3 in volume were used for the experiments. Tumor volumes were calculated from the greatest longitudinal diameter (length) and the greatest transverse diameter (width) using the following formula; tumor volume = length × $width^2$ × 0.5, based on caliper measurements. Mice were monitored each day, and tumor volumes were measured three times a week for MC38-luc and LL/2 tumors and twice a week for MOC1 tumors until the tumor volume reached 2,000 mm^3, whereupon the mice were euthanized with inhalation of carbon dioxide gas. Tumor disappearance for 4 weeks or longer after treatment was defined as complete remission.

In vivo bioluminescence imaging and IR700 fluorescence imaging

To obtain bioluminescence images in MC38-luc tumor-bearing mice, D-luciferin (15 mg/mL, 150 μL, Goldbio) was intraperitoneally injected to mice. Luciferase activity was analyzed with a bioluminescence imaging system (Photon Imager; Biospace Lab, Paris, France) using relative light units. Regions of interests (ROIs) were placed over the entire tumor. The counts per minute of relative light units were calculated using M3 Vision Software (Biospace Lab) and converted to the percentage based on those before NIR-PIT using the following formula: ((relative light units after treatment) / (relative light units before treatment) × 100 (%)) [27]. Bioluminescence imaging was performed before and after NIR-PIT (protocol below) on day 0 to day 7.

In vivo fluorescence imaging studies

Tumor bearing mice were imaged after tumors reached volumes of approximately 150 mm^3. Serial dorsal fluorescence images of the IR700 signal were obtained with a Pearl Imager (LI-COR Biosciences) using a 700-nm fluorescence channel 1, 4, 6, 12, 24, and 48 hours after intravenous injection of 100 μg of anti-CD25-IR700 via the tail vein. ROIs were placed on the tumor and the adjacent non-tumor region as background. The mean value of fluorescence intensity was calculated for each ROI. Target-to-background ratio was calculated from fluorescence intensities of tumors and fluorescence intensity of background by the following formula: (mean fluorescence intensity of tumor) – (mean fluorescence intensity of background) / (mean fluorescence intensity of background).

Immunohistochemistry staining

Immunohistochemistry assays for CD44 was performed using BOND RXm automated stainer (Leica Biosystems). The paraffin-embedded tumor samples were sliced into 4 μm

thickness. Dewaxed sections were incubated in BOND ER2 solution (EDTA-based, pH 9.0, Leica Biosystems) at 95˚C for 20 minutes, followed by incubation with anti-CD44 (clone IM7, BioXcell, 1:5000 dilution) and ImmPRESS HRP Anti-Rat IgG (Peroxidase) Polymer Detection Kit (Vector laboratories). Visualization by DAB and counterstain with hematoxylin were performed using the Bond Polymer Refine Detection kit (Leica Biosystems, Wetzlar, Germany) according to the manufacturer's instructions. Stained slides were mounted with Permount mounting medium (Fisher Scientific) and then pictures were taken using Mantra Quantitative Pathology Workstation (Perkin Elmer).

Multi-color immunofluorescence

Multi-color immunofluorescence for tumor-infiltrating lymphocytes (TILs) in tissue sections was performed using Opal 7-Color Automation IHC Kit (Akoya Bioscience, Hopkinton, MA, USA) and BOND RXm auto stainer (Leica Biosystems). The following antibodies were used: anti-CD8 (clone EPR20305, Abcam, 1:500 dilution), anti-CD4 (clone EPR19514, Abcam, 1:1000 dilution), anti-FoxP3 (clone 1054C, Novus Biologicals, 1:1000 dilution), anti-pan cytokeratin (rabbit poly, Bioss, 1:500 dilution). The staining was performed according to the Opal 7 color protocol provided by manufacturer with following modification: (i) antigen retrieval was performed using BOND ER2 solution (Leica Biosystems) for 20 minutes and (ii) the ImmPRESS HRP anti-Rabbit IgG (Peroxidase) Polymer Detection Kit (Vector laboratories) was used instead of anti-mouse/human secondary antibody provided in the kit. Stained slides were mounted with VECTASHIELD Hardset Antifade Mounting Medium (Vector laboratories) then imaged using Mantra Quantitative Pathology Workstation (Perkin Elmer). Images were analyzed with inForm software (Akoya Biosystems). InForm software was trained to automatically detect tissues and cell phenotype according to following criteria: areas with pan-cytokeratin expression = tumor, other areas = stroma, $CD4^+FoxP3^+$ cells = Treg, $CD8^+$ or $CD4^+$ = $CD8^+$ or $CD4^+$ T cells, respectively. Cell count of each phenotype was exported and shown as count per megapixel area. Three tumor samples were tested for each group. Five pictures were taken for each specimen, and cell count and tissue area were combined for all five pictures.

NIR-PIT

The mice with tumors that reached volumes of approximately 150 mm^3 were selected and divided randomly into 4 experimental groups for the following treatments: (i) no treatment (control); (ii) intravenous injection of 100 μg anti-CD25-IR700, followed by external NIR light irradiation at 100 J/cm^2 on day 0 (CD25-targeted NIR-PIT); (iii) intravenous injection of 100 μg anti-CD44-IR700, followed by external NIR light irradiation at 100 J/cm^2 on day 0 (CD44-targeted NIR-PIT); and (iv) intravenous injection of 50 μg anti-CD25-IR700 and 50 μg anti-CD44-IR700, followed by external NIR light irradiation at 100 J/cm^2 on day 0 (combined NIR-PIT). For the mice with MC38-luc tumors, LL/2 tumors, and MOC1 tumors in the NIR-PIT–treated groups, IV injection of the antibody–photo-absorber conjugates was performed 5, 5, and 28 days after tumor inoculation, respectively, followed by external NIR light irradiation at 100 J/cm^2 1 day after injection. NIR light was administered to tumor-bearing mice using a red light–emitting diode (LED), which emits light in the range of 670 to 710 nm (L690–66-60; Marubeni America Co.) at a power density of 50 mW/cm^2 as measured with an optical power meter (PM 100, Thorlabs). IR700 absorbs light at

approximately 690 nm. IR700 fluorescence images were obtained before and after NIR light irradiation at the timepoints indicated in each experiment.

Flow cytometric analysis after NIR-PIT

MC38-luc tumors or regional lymph nodes (LNs) were harvested after NIR-PIT at various timepoint indicated in each experiment. Single-cell suspensions from tumor samples were prepared using following protocol. Whole tumors were incubated in the DMEM media (Thermo Fisher Scientific) containing collagenase type IV (1 mg/mL, Worthington biochemical) and DNaseI (20 μg/mL, Millipore Sigma) in 37˚C for 30 minutes, then gently mashed with the back of the plunger of 3 mL syringe. The tissues were passed through 70-mm mesh filters by pipetting. 1.0×10^6 cells were stained and data for 1.0×10^5 cells were collected for each tumor. The cells were stained with following antibodies: anti-CD3e (clone 145–2C11), anti-CD4 (clone RM4–5), anti-CD25 (clone 3C7), anti-CD11b (clone M1/70), and anti-MHCII (clone 10–3.6) were obtained from Biolegend; anti-CD11c (clone N418), anti-CD69 (clone H1.2F3), anti-Foxp3 (clone FJK-16s), and anti-IFNγ (clone XMG1.2) were obtained from eBioscience.. Foxp3 was stained after fixation and permeabilization using the Foxp3 Transcription Factor Staining Buffer Set (eBioscience). For IFNγ staining, cells were cultured with or without stimulation with cell activation cocktail containing PMA and ionomycin (81 nM and 1.3 μM, respectively, Biolegend) for 4 hours in medium supplemented with brefeldin A (5 μg/mL, Biolegend), followed by fixation/permeabilization with Intracellular Fixation & Permeabilization Buffer Set (eBioscience) before the anti-IFNγ staining. The stained cells were analyzed in a FACS Calibur flow cytometer (BD), and data were analyzed with the FlowJo software (FlowJo, LLC). Dead cells were removed from analysis based on fsc, ssc and staining with LIVE/DEAD Fixable Dead Cell Stain (ThermoFisher Scientific). Treg population was defined by gating for $CD25^+Foxp3^+$ cells among $CD3e^+CD4^+$ cells.

Statistical Analysis

Quantitative data were expressed as means ± standard error of the mean (SEM). The Mann-Whitney U Test was used to compare differences between two groups. For multiple comparisons (≥3 groups), a one-way analysis of variance (ANOVA) followed by the Tukey-Kramer test was used. The cumulative probability of survival was analyzed by the Kaplan-Meier survival curve analysis, and the results were compared with the Log-rank test. Statistical analysis was performed with JMP 13 software (SAS Institute) or Prism software (GraphPad). A p value of less than 0.05 was considered significant.

Results

In vivo fluorescence imaging after administration of anti-CD25-IR700

High fluorescence intensity was observed in MC38-luc, LL/2, and MOC1 tumors one hour after anti-CD25-IR700 injection, and fluorescence in all tumor types gradually increased until 24 hours post injection (Figure 1A-B). The fluorescence intensity 48 hours after injection decreased compared to the fluorescence intensity at 24 hours. The target-to-background ratio of anti-CD25-IR700 in all tumor types also gradually increased until 24 hours and decreased 48 hours after injection (Figure 1C). The highest mean fluorescence

intensity and target-to-background ratio were observed 24 hours after injection. MC38-luc and LL/2 tumors showed higher mean fluorescence intensity and target-to-background ratio than MOC1 tumors (Figure 1B-C). These data demonstrated the delivery of therapeutic NIR light exposure 1 day after injection of the antibody–photo-absorber conjugate for both CD25- and/or CD44-targeted NIR-PIT.

Comparison of CD44 expression among MC38-luc, LL/2, and MOC1 tumors

To compare differences in CD44 expression *in vivo* among different types of tumors, size-matched MC38-luc, LL/2, and MOC1 tumors were assessed by means of immunohistochemistry staining (Figure 2A-C). CD44 expression within the tumors was observed in MC38-luc and LL/2 tumors, which expressed greater CD44 compared to MOC1 tumors. This suggested whole tumor accumulation of anti-CD44-IR700 1 day after injection as a target antigen was lower in MOC1 tumors compared with MC38-luc or LL/2 tumors.

CD25-targeted NIR-PIT induces selective and effective depletion of Tregs

To verify the effect of *in vivo* local CD25-targeted NIR-PIT with anti-CD25-IR700 against $FOXP3^+CD25^+CD4^+$ Tregs within tumors, MC38-luc tumors were harvested 1 day after NIR-PIT and were assessed for Treg depletion via flow cytometry (Figure 3A-B). $FOXP3^+CD25^+CD4^+$ Treg counts in MC38-luc tumors treated both with CD25-targeted NIR-PIT and with combined NIR-PIT showed significantly lower counts compared to those without treatment (Figure 3A-B). These data demonstrated CD25-targeted NIR-PIT is effective in depleting $FOXP3^+CD25^+CD4^+$ Treg populations.

Combined CD44- and CD25-targeted NIR-PIT induces activation of $CD8^+$ T cells

In order to investigate how combined CD44- and CD25-targeted NIR-PIT activated antitumor immunity, we examined if intratumoral $CD8^+$ T cells were activated after NIR-PIT. Tumors or regional LNs in MC38-luc tumor-bearing mice were harvested 3 hours, 1 day, and 2 days after NIR-PIT to assess $CD8^+$ T-cell activation at early stages via flow cytometry. Intratumoral $CD8^+$ T cells 1 day after combined NIR-PIT showed significantly higher IFNγ production compared to control tumors, although it was seen 3 hours after NIR-PIT (Supplementary Figure S1). Two days after NIR-PIT, a significant increase in $CD8^+$ T cells producing IFNγ and expressing upregulated activation marker CD69 were identified within the tumors treated with combined NIR-PIT (Supplementary Figure S1). These data suggested that the combined CD44- and CD25-targeted NIR-PIT induced activation of $CD8^+$ T cells in TME.

In the regional LNs, we examined if dendritic cells (DCs) were activated after NIR-PIT. DCs in TME are known to migrate to regional LNs upon their activation then activate $CD8^+$ T cells. Conventional type-1 DCs (cDC1s) are thought to have major role inthis process [28]. cDC1s are included in the $CD11b^{low}CD11c^+$ population and activated DCs express MHCII. In the regional LNs, we observed a significant increase of $MHCII^+$ cells within $CD11b^{low}CD11c^+$ cells 3 hours after combined NIR-PIT. A slight increase of MHCII expression was observed in $CD11b^{hi}CD11c^+$ population. cDC2s are thought to have minor roles in TIL activation (Supplementary Figure S2). These results suggested that the $CD8^+$

T-cell activation after combined NIR-PIT was induced through rapid DC maturation in the regional LNs.

To assess durable TIL infiltration into tumors, MC38-luc tumors 7 days after NIR-PIT were harvested for immunohistochemistry analysis. In order to evaluate $CD4^+$ T cells, $CD8^+$ T cells, and Tregs within tumors quantitatively, cell counts per megapixel in immunofluorescence images were performed and compared among control, CD25-targeted NIR-PIT, CD44-targeted NIR-PIT, and combined NIR-PIT groups. Cell counts of tumor-infiltrating $CD8^+$ T cells in the combined NIR-PIT group showed significantly higher infiltration than the other groups (Figure 3C-D). This result suggested that $CD8^+$ T-cell infiltration into tumors was significantly enhanced with the combination of CD44- and CD25-targeted NIR-PIT. On the other hand, no significant difference in $CD8^+$ T-cell counts within stromal tissues was seen, which underscores the importance of tumor-infiltrating $CD8^+$ T cells for durable host antitumor immune responses.

Efficacy of combined CD44- and CD25-targeted NIR-PIT for MC38-luc tumors

MC38 tumors have high CD44 expression on the cell membrane (Figure 2), also known to have relatively high $CD8^+$ T-cell infiltration compared to LL/2 and MOC1 tumors [29,30]. The NIR-PIT regimen and imaging protocol are depicted in Figure 4A. One day after injection of anti-CD25- and/or anti-CD44-IR700, the tumors were exposed to NIR light via LED light. IR700 fluorescence signal in tumors decreased due to dispersion of fluorophore from dying cells and partial photo-bleaching in all cases (Figure 4B). To investigate tumor-killing efficacy after NIR-PIT, bioluminescence imaging was performed before and after NIR-PIT up to day 7 (Figure 4C). In most mice, in the NIR-PIT–treated groups, luciferase activity decreased shortly after NIR-PIT and then gradually increased (Figure 4C). This change pattern in luciferase activity was likely due to a large amount of initial cancer cell killing, followed by slower outgrowth of cells not originally killed. In contrast, in some mice in the CD25-targeted NIR-PIT and combined NIR-PIT groups, luciferase activity decreased shortly after NIR-PIT and disappeared thereafter (Figure 4C). This change in luciferase activity was likely due to a large amount of initial cancer cell killing, followed by complete remission of treated tumors due to an enhanced immune response. Luciferase activity after treatment in all NIR-PIT–treated groups was significantly lower at all time points after NIR-PIT than in the control group (Figure 4D). Combined CD44- and CD25-targeted NIR-PIT showed significantly lower luciferase activity 7 days after NIR-PIT compared with CD44-targeted NIR-PIT alone (Figure 4D). Tumor volume in all the NIR-PIT–treated groups was significantly inhibited 5, 7, and 10 days after NIR-PIT compared to the control group (Figure 4E), but the combined CD44- and CD25-targeted NIR-PIT showed significantly greater tumor reduction compared to CD44-targeted NIR-PIT alone at 7 and 10 days after NIR-PIT (Figure 4E). No significant tumor inhibition was observed in the other groups. These data showed that combined CD44- and CD25-targeted NIR-PIT led to the slowest rate of tumor regrowth compared with other NIR light exposure groups.

Combined CD44- and CD25-targeted NIR-PIT also was associated with significantly prolonged survival compared with CD25-targeted NIR-PIT alone and CD44-targeted NIR-

PIT alone (Figure 4F). Two of 15 mice in the CD25-targeted NIR-PIT group and 9 of 14 mice in the combined NIR-PIT group achieved complete remission after a single round of NIR-PIT. Our results showed that combined CD44- and CD25-targeted NIR-PIT enables superior *in vivo* therapeutic responses compared to the other two monotherapies of NIR-PIT for MC38-luc tumors.

Efficacy of combination CD44- and CD25-targeted NIR-PIT for LL/2 tumor

LL/2 tumors have high CD44 expression on the cell membrane (Figure 2) but known to have relatively low $CD8^+$ T-cell infiltration compared to MC38 tumors [28]. The NIR-PIT regimen and imaging protocol are depicted in Figure 5A. One day after injection of anti-CD25- and/or anti-CD44-IR700, the tumors were exposed to NIR light. IR700 tumor fluorescence signal decreased due to dispersion of fluorophore from dying cells and partial photo-bleaching (Figure 5B). Tumor volume in all the NIR-PIT–treated groups was significantly inhibited 5, 7, 10, and 12 days after NIR-PIT compared to the control group (Figure 5C). Among the three NIR-PIT–treated groups, combined CD44- and CD25-targeted NIR-PIT showed significantly greater tumor reduction compared to CD44-targeted NIR-PIT alone 17 days after NIR-PIT (Figure 5C). In the long-term follow-up, mice treated with combined CD44- and CD25-targeted NIR-PIT had significantly prolonged survival compared to those treated with CD25-targeted NIR-PIT alone or CD44-targeted NIR-PIT alone (Figure 5D). In 3 of 9 mice in the combined NIR-PIT group, complete remission of tumors was achieved after only a single round of NIR-PIT. Thus, combined CD44- and CD25-targeted NIR-PIT was therapeutically superior to the other two single target NIR-PITs in LL/2 tumors.

Efficacy of combined CD44- and CD25-targeted NIR-PIT for MOC1 tumors

MOC1 tumors have extremely low CD44 expression on the cell membrane (Figure 2) and baseline expression of tumor-associated antigens is low relative to MC38 and LL/2 [14]. The NIR-PIT regimen and imaging protocol are depicted in Figure 6A. One day after injection of anti-CD25- and/or anti-CD44-IR700, the tumors were exposed to NIR light. IR700 tumor fluorescence signal decreased due to dispersion of fluorophore from dying cells and partial photo-bleaching (Figure 6B). Tumor volume in all the NIR-PIT–treated groups was significantly inhibited at all time points after NIR-PIT compared to the control group (Figure 6C). Combined CD44- and CD25-targeted NIR-PIT showed significantly greater tumor reduction 28 days after NIR-PIT compared to CD44-targeted NIR-PIT. In the long-term follow-up, mice administered combined CD44- and CD25-targeted NIR-PIT showed significantly prolonged survival compared to those that received CD44-targeted NIR-PIT (Figure 6D). On the other hand, no significant difference in tumor volume and survival between CD25-targeted NIR-PIT alone and CD44-targeted NIR-PIT alone, and between CD25-targeted NIR-PIT alone and the combined NIR-PIT was seen (Figure 6D). One of 9 mice in the combined NIR-PIT group achieved complete remission after a single round of NIR-PIT. Combined CD44- and CD25-targeted NIR-PIT was superior therapeutically to CD44-targeted NIR-PIT alone in MOC1 tumors but did not exhibit significantly greater benefit compared to CD25-targeted NIR-PIT.

Discussion

A variety of new cancer treatment strategies rely on enhancing immune cell function against tumors using, for instance, immune checkpoint inhibitors and immunosuppressive cell-depleting drugs. Although these approaches demonstrably enhance immune responses, they have not always resulted in clinically meaningful outcomes. In order to improve therapeutic efficacy, cancer therapies must combine direct tumor cell killing and enhanced antitumor immunity. NIR-PIT is a new therapy that can selectively kill cancer cells by targeting tumor antigens and also simultaneously eliminate immunosuppressive cells, such as Tregs, to optimize integrated “cancer” and “immune” therapy. We selected CD44 and CD25 as targets for cancer and Treg cells, respectively, in this study because they are versatile targets in a variety of tumors.

In order for NIR PIT to be successful, there must be adequate accumulation and retention of the antibody–photo-absorber conjugate within targeted tumors. The pharmacokinetics of the anti-CD44-IR700 has been previously reported and requires approximately 24 hours to accumulate in the tumor after intravenous injection [13]. *In vivo* IR700 fluorescence after administration of anti-CD25-IR700 showed selective uptake in the targeted tumors. The conjugation of IR700 to the anti-CD25 and CD44 minimally alters the pharmacokinetics of the unconjugated antibody alone. Thus, both anti-CD44- and anti-CD25-IR700 have predictable uptake in target tumors.

CD44-IR700 NIR-PIT targets a cancer antigen and initiates necrotic and immunogenic cell death [3], unlike apoptotic cell death that most other cancer therapies induce [31]. Selective immunogenic cell death of cancer cells releases damage-associated signals, including adenosine triphosphate (ATP), calreticulin and high mobility group box 1 (HMGB1), that promote maturation of immature DCs adjacent to dying cancer cells. Cell membrane rupture after NIR-PIT releases tumor-specific antigens in their intact forms into the TME. Therefore, antigen-presenting mature DCs process and present cancer-specific antigens to naive T cells for priming [3,14,32]. However, in some syngeneic mouse models, $FOXP3^+CD25^+CD4^+$ Tregs suppress host antitumor immunity by inhibiting DC function through the CTLA4 axis or effector T or NK cell activation [33–35]. $FOXP3^+CD25^+CD4^+$ Tregs have been reported to be better at recognizing tumor-associated antigens because their T-cell receptor repertoires are more self-reactive than conventional T cells and they have higher expression of T-cell accessory molecules [36,37]. Increased exposure to tumor antigens in the TME in the presence of Tregs may preferentially activate antigen-specific Tregs rather than antigen-specific effector T cells [38]. To overcome this, we proposed simultaneously targeting cancer cells and Tregs using combined CD44- and CD25-targeted NIR-PIT, which resulted in superior antitumor effects and prolonged survival compared to NIR-PIT using either target alone. In comparison, CD44-targeted NIR-PIT alone was less effective in all three syngeneic tumor models investigated. Although Tregs mediate tumor immune escape using various immunosuppressive mechanisms, CD25-targeted NIR-PIT can disable these mechanisms through selective Treg depletion. Our results suggested that combined NIR-PIT resulted in superior *in vivo* therapeutic benefits over conventional cancer antigen-targeted NIR-PIT or elimination of immunosuppressive cell function alone.

Combined CD44- and CD25-targeted NIR-PIT prolonged survival compared to CD25-targeted NIR-PIT alone in both MC38-luc and LL/2 models. This suggests that adding cancer antigen-targeted NIR-PIT to Treg depletion is associated with improved long-term outcome. Indeed, successful depletion of $FOXP3^+CD25^+CD4^+$ Tregs restores local antitumor immunity [23], but its efficacy is limited in the absence of localized immunogenic death of tumor cells and subsequent antigen release and processing. In contrast, cancer antigen-targeted NIR-PIT induces tumor cell killing both directly and by activation of host immune cells, resulting in rapid reduction of tumor viability after NIR light exposure [13,14]. Immunogenic cell death enhances immunogenicity through increased exposure to tumor-specific antigens, which acts as a trigger of DC maturation promoting activation of antitumor effector cells, especially tumor-infiltrating $CD8^+$ T cells. It is important for long-term tumor control to provoke immunogenic cell death with tumor antigen-targeted NIR-PIT, which was increased when Tregs were also targeted. However, this effect was not present in all tumor types. For instance, combined CD44- and CD25-targeted NIR-PIT did not show significantly prolonged survival compared to CD25-targeted NIR-PIT alone in the MOC1 model. In our study, MOC1 tumors showed lower CD44 expression than MC38-luc and LL/2 tumors, yet the infiltration of $CD8^+$ T cells into MOC1 tumors was similar to that in MC38 or LL/2 tumors [29,30]. Our previous study also demonstrated that there was no significant increase in tumor MHC class II^+ DCs or lymphocyte infiltration following CD44-targeted NIR-PIT of MOC1 tumors as there was in LL/2 and MC38, indicating a lack of DC priming [14]. Therefore, CD44 expression within tumors can be one of factors related to therapeutic effects with combined NIR-PIT. An alternative cell surface marker may be needed for successful NIR-PIT in tumors with low CD44 expression. However, variation of immune cell composition in different types of tumors could also affect treatment outcome with combined NIR-PIT. Further research would require elucidation of the association between therapeutic effects with NIR-PIT and immune cell composition among the different tumor types.

Complete remission of tumors was observed in several mice but only after a single round of combined CD44- and CD25-targeted NIR-PIT. This occurred in all three types of tumors but not in every mouse, indicating variability in immune responses. In those tumors in which it occurred, long-term antitumor immunity was achieved by combined NIR-PIT. The presence of $FOXP3^+CD25^+CD4^+$ Tregs has been reported to hinder development of tumor-specific, high-avidity effector T cells, although low-avidity effector T cells can function and expand [39,40]. Immunogenic cell death by CD44-targeted NIR-PIT induces DC maturation [3], and Treg depletion enables activation and expansion of tumor-specific, high-avidity T cells from naive T-cell precursors, allowing their differentiation into high-avidity effector T cells capable of mediating potent antitumor immune responses [33]. When this occurs, long-term antitumor immunity might be induced due to activation of tumor-specific, high-avidity effector or memory T cells (Figure 7). NIR-PIT can be repeatedly performed because it causes minimal damage to surrounding normal adjacent cells [1,4]. Repeated NIR-PIT has been previously reported to improve efficacy of NIR-PIT [41,42], increasing the frequency of complete remission in targeted tumors.

Currently, a Phase III clinical trial of NIR-PIT using cetuximab-IR700 for head and neck cancer patients is underway. In Phase I/II studies, to overcome limited depth of penetration

by NIR light in tissue, cylindrical diffusing optical fibers are inserted in the tumor to deliver light throughout the tumor [43,44]. Both anti-human CD44 (RG7356) and anti-human CD25 (basiliximab or daclizumab) have been approved by the FDA. Thus, clinical translation of the combined NIR-PIT regimen performed in this study is possible, which may permit extension of NIR-PIT to a range of cancer types in a variety of anatomic locations.

Besides NIR-PIT, another approach utilizing light to treat cancer called photodynamic therapy (PDT) has been reported [45]. NIR-PIT differs from PDT in several aspects. First, in NIR-PIT, cell killing is selectively induced to cells that antibody–photo-absorber conjugates bind based on the unique photo-induced ligand release reaction rather than reactive oxygen species production [46]. Second NIR-PIT rationally induces rapid and effective activation of antitumor host immunity due to selective immunogenic cell death in targeted cancer cells [3,14], whereas such effects are not generally induced by non-selective cell killing with PDT.

This study had several limitations. First, we used subcutaneously xenografted tumor models to evaluate the therapeutic effects of NIR-PIT. Although an orthotopic tumor model may be more clinically relevant because the TME is more realistic [47], we chose a model in which each tumor had a consistent size, shape, and location for comparing *in vivo* therapeutic efficacy. The orthotopic model also requires substantial surgical skill for proper implanting of the tumor. Second, we used anti-CD25-IgG to conjugate to IR700, although anti-CD25-F(ab′)$_2$-IR700 was used previously [23]. Both activated effector T cells and FOXP3$^+$CD25$^+$CD4$^+$ Tregs express CD25 on the cell membrane, where it is part of the IL2 binding complex that activates and causes replication of effector T cells. Therefore, anti-CD25-IgG–based cell depletion with NIR-PIT can theoretically reduce activated effector T cell function by blocking IL2 binding or by induction of antibody-dependent cellular cytotoxicity, potentially reducing antitumor efficacy. Anti-CD25-F(ab′)$_2$-based NIR-PIT is theoretically a better approach than anti-CD25-IgG-based NIR-PIT due to superior effector T-cell activation. However, production of the F(ab')2 antibody fragments is cumbersome and can give low yield, which is not cost effective for massive production, hindering clinical translation of its use in NIR-PIT. In this study, CD44- and CD25- targeted NIR-PIT using anti-CD25-IgG-IR700 showed superior therapeutic effects to CD44-targeted NIR-PIT alone in the three mouse models, suggesting that inhibited proliferation of effector T cells due to blocking IL2 binding by anti-CD25 IgG-IR700 is not critical compared to the overall activating immunity of this combined regimen. Third, there were variations among the experimental protocols for each tumor model used in this study. This included numbers of tumor cells for each model and timepoints of tumor measurement due to the slow growth of MOC1 tumors and protocols previously used for the model [13, 14]. However, we conclude that the variation of experimental protocol for each tumor in this study does not affect the results.

In conclusion, combined CD44- and CD25-targeted NIR-PIT showed superior *in vivo* therapeutic efficacy to either CD44- or CD25-targeted NIR-PIT alone. This combined regimen of NIR-PIT is an effective method, especially for tumors with high target antigen expression and with abundant Tregs, to induce long-term antitumor immunity because:(i) Direct tumor cell killing induced by cancer antigen-targeted NIR-PIT; (ii) Host immunity

initiated by immunogenic cell death; and (iii) Effective activation of naïve and acquired antitumor immune immunity induced by selective Treg depletion. These three events, working together have potential to elicit long-term tumor responses in otherwise resistant tumors.

Supplementary Material

Refer to Web version on PubMed Central for supplementary material.

Acknowledgement

This research was supported by the Intramural Research Program of the National Institutes of Health, National Cancer Institute, Center for Cancer Research (ZIA BC011513).

Financial Support

All authors were supported by the Intramural Research Program of the NIH, NCI, Center for Cancer Research (ZIA BC011513).

References

1. Mitsunaga M, Ogawa M, Kosaka N, Rosenblum LT, Choyke PL, Kobayashi H. Cancer cell-selective in vivo near infrared photoimmunotherapy targeting specific membrane molecules. Nat Med2011;17:1685–91. [PubMed: 22057348]
2. Bezu L, Gomes-de-Silva LC, Dewitte H, Breckpot K, Fucikova J, Spisek R, et al.Combinatorial strategies for the induction of immunogenic cell death. Front Immunol2015;6:187. [PubMed: 25964783]
3. Ogawa M, Tomita Y, Nakamura Y, Lee MJ, Lee S, Tomita S, et al.Immunogenic cancer cell death selectively induced by near infrared photoimmunotherapy initiates host tumor immunity. Oncotarget2017;8:10425–36. [PubMed: 28060726]
4. Mitsunaga M, Nakajima T, Sano K, Kramer-Marek G, Choyke PL, Kobayashi H. Immediate in vivo target-specific cancer cell death after near infrared photoimmunotherapy. BMC Cancer2012;12:345. [PubMed: 22873679]
5. Sato K, Nakajima T, Choyke PL, Kobayashi H. Selective cell elimination in vitro and in vivo from tissues and tumors using antibodies conjugated with a near infrared phthalocyanine. RSC Adv2015;5:25105–14. [PubMed: 25866624]
6. Muntimadugu E, Kumar R, Saladi S, Rafeeqi TA, Khan W. CD44 targeted chemotherapy for co-eradication of breast cancer stem cells and cancer cells using polymeric nanoparticles of salinomycin and paclitaxel. Colloids Surf B Biointerfaces2016;143:532–46. [PubMed: 27045981]
7. Ponta H, Sherman L, Herrlich PA. CD44: from adhesion molecules to signalling regulators. Nat Rev Mol Cell Biol2003;4:33–45. [PubMed: 12511867]
8. Tovuu LO, Imura S, Utsunomiya T, Morine Y, Ikemoto T, Arakawa Y, et al.Role of CD44 expression in non-tumor tissue on intrahepatic recurrence of hepatocellular carcinoma. Int J Clin Oncol2013;18:651–6. [PubMed: 22706704]
9. Naor D, Nedvetzki S, Golan I, Melnik L, Faitelson Y. CD44 in cancer. Crit Rev Clin Lab Sci2002;39:527–79. [PubMed: 12484499]
10. Chen J, Zhou J, Lu J, Xiong H, Shi X, Gong L. Significance of CD44 expression in head and neck cancer: a systemic review and meta-analysis. BMC Cancer2014;14:15. [PubMed: 24410905]
11. de Jong MC, Pramana J, van der Wal JE, Lacko M, Peutz-Kootstra CJ, de Jong JM, et al.CD44 expression predicts local recurrence after radiotherapy in larynx cancer. Clin Cancer Res2010;16:5329–38. [PubMed: 20837694]
12. Motegi A, Fujii S, Zenda S, Arahira S, Tahara M, Hayashi R,et al.Impact of Expression of CD44, a Cancer Stem Cell Marker, on the Treatment Outcomes of Intensity Modulated Radiation

Therapy in Patients With Oropharyngeal Squamous Cell Carcinoma. Int J Radiat Oncol Biol Phys2016;94:461–8. [PubMed: 26867875]

13. Nagaya T, Nakamura Y, Okuyama S, Ogata F, Maruoka Y, Choyke PL, et al.Syngeneic Mouse Models of Oral Cancer Are Effectively Targeted by Anti-CD44-Based NIR-PIT. Mol Cancer Res2017;15:1667–77. [PubMed: 28923838]
14. Nagaya T, Friedman J, Maruoka Y, Ogata F, Okuyama S, Clavijo PE, et al.Host Immunity Following Near-Infrared Photoimmunotherapy Is Enhanced with PD-1 Checkpoint Blockade to Eradicate Established Antigenic Tumors. Cancer Immunol Res. 2019;7:401–413. [PubMed: 30683733]
15. Sakaguchi S, Sakaguchi N, Shimizu J, Yamazaki S, Sakihama T, Itoh M, et al.Immunologic tolerance maintained by $CD25^+$ $CD4^+$ regulatory T cells: their common role in controlling autoimmunity, tumor immunity, and transplantation tolerance. Immunol Rev2001;182:18–32. [PubMed: 11722621]
16. Shevach EM, DiPaolo RA, Andersson J, Zhao DM, Stephens GL, Thornton AM. The lifestyle of naturally occurring $CD4^+$ $CD25^+$ $Foxp3^+$ regulatory T cells. Immunol Rev2006;212:60–73. [PubMed: 16903906]
17. Kretschmer K, Apostolou I, Jaeckel E, Khazaie K, von Boehmer H. Making regulatory T cells with defined antigen specificity: role in autoimmunity and cancer. Immunol Rev2006;212:163–9. [PubMed: 16903913]
18. Vignali DA, Collison LW, Workman CJ. How regulatory T cells work. Nat Rev Immunol2008;8:523–32. [PubMed: 18566595]
19. Curiel TJ, Coukos G, Zou L, Alvarez X, Cheng P, Mottram P, et al.Specific recruitment of regulatory T cells in ovarian carcinoma fosters immune privilege and predicts reduced survival. Nat Med2004;10:942–9. [PubMed: 15322536]
20. Zou W. Regulatory T cells, tumour immunity and immunotherapy. Nat Rev Immunol2006;6:295–307. [PubMed: 16557261]
21. Ko K, Yamazaki S, Nakamura K, Nishioka T, Hirota K, Yamaguchi T, et al.Treatment of advanced tumors with agonistic anti-GITR mAb and its effects on tumor-infiltrating $Foxp3^+CD25^+CD4^+$ regulatory T cells. J Exp Med2005;202:885–91. [PubMed: 16186187]
22. Sugiyama D, Nishikawa H, Maeda Y, Nishioka M, Tanemura A, Katayama I, et al.Anti-CCR4 mAb selectively depletes effector-type $FoxP3^+CD4^+$ regulatory T cells, evoking antitumor immune responses in humans. Proc Natl Acad Sci USA2013;110:17945–50. [PubMed: 24127572]
23. Sato K, Sato N, Xu B, Nakamura Y, Nagaya T, Choyke PL, et al.Spatially selective depletion of tumor-associated regulatory T cells with near-infrared photoimmunotherapy. Sci Transl Med2016;8:352ra110.
24. Ito K, Mitsunaga M, Nishimura T, Kobayashi H, Tajiri H. Combination photoimmunotherapy with monoclonal antibodies recognizing different epitopes of human epidermal growth factor receptor 2: an assessment of phototherapeutic effect based on fluorescence molecular imaging. Oncotarget2016;7:14143–52. [PubMed: 26909859]
25. Nagaya T, Okuyama S, Ogata F, Maruoka Y, Choyke PL, Kobayashi H. Endoscopic near infrared photoimmunotherapy using a fiber optic diffuser for peritoneal dissemination of gastric cancer. Cancer Sci2018;109:1902–8. [PubMed: 29676827]
26. Nishikawa H, Sakaguchi S. Regulatory T cells in tumor immunity. Int J Cancer2010;127:759–67. [PubMed: 20518016]
27. Maruoka Y, Nagaya T, Nakamura Y, Sato K, Ogata F, Okuyama S, et al.Evaluation of Early Therapeutic Effects after Near-Infrared Photoimmunotherapy (NIR-PIT) Using Luciferase-Luciferin Photon-Counting and Fluorescence Imaging. Mol Pharm2017;14:4628–35. [PubMed: 29135265]
28. Fu C, Jiang A. Dendritic Cells and CD8 T Cell Immunity in Tumor Microenvironment. Front Immunol. 2018;9:3059. [PubMed: 30619378]
29. Mosely SI, Prime JE, Sainson RC, Koopmann JO, Wang DY, Greenawalt DM, et al.Rational Selection of Syngeneic Preclinical Tumor Models for Immunotherapeutic Drug Discovery. Cancer Immunol Res. 2017;5:29–41. [PubMed: 27923825]

30. Davis RJ, Moore EC, Clavijo PE, Friedman J, Cash H, Chen Z, et al.Anti-PD-L1 Efficacy Can Be Enhanced by Inhibition of Myeloid-Derived Suppressor Cells with a Selective Inhibitor of PI3Kδ/γ. Cancer Res. 2017;77:2607–19. [PubMed: 28364000]
31. Evan GI, Vousden KH. Proliferation, cell cycle and apoptosis in cancer. Nature2001;411:342–8. [PubMed: 11357141]
32. Inoue H, Tani K. Multimodal immunogenic cancer cell death as a consequence of anticancer cytotoxic treatments. Cell Death Differ2014;21:39–49. [PubMed: 23832118]
33. Nishikawa H, Sakaguchi S. Regulatory T cells in cancer immunotherapy. Curr Opin Immunol2014;27:1–7. [PubMed: 24413387]
34. Tang Q, Adams JY, Tooley AJ, Bi M, Fife BT, Serra P, et al.Visualizing regulatory T cell control of autoimmune responses in nonobese diabetic mice. Nat Immunol2006;7:83–92. [PubMed: 16311599]
35. Tadokoro CE, Shakhar G, Shen S, Ding Y, Lino AC, Maraver A, et al.Regulatory T cells inhibit stable contacts between $CD4^+$ T cells and dendritic cells in vivo. J Exp Med2006;203:505–11. [PubMed: 16533880]
36. Jordan MS, Boesteanu A, Reed AJ, Petrone AL, Holenbeck AE, Lerman MA, et al.Thymic selection of $CD4^+CD25^+$ regulatory T cells induced by an agonist self-peptide. Nat Immunol2001;2:301–6. [PubMed: 11276200]
37. Sakaguchi S. Naturally arising $CD4^+$ regulatory t cells for immunologic self-tolerance and negative control of immune responses. Annu Rev Immunol2004;22:531–62. [PubMed: 15032588]
38. Francois V, Ottaviani S, Renkvist N, Stockis J, Schuler G, Thielemans K, et al.The CD4(+) T-cell response of melanoma patients to a MAGE-A3 peptide vaccine involves potential regulatory T cells. Cancer Res2009;69:4335–45. [PubMed: 19435913]
39. Nishikawa H, Jager E, Ritter G, Old LJ, Gnjatic S. $CD4^+$ $CD25^+$ regulatory T cells control the induction of antigen-specific $CD4^+$ helper T cell responses in cancer patients. Blood2005;106:1008–11. [PubMed: 15840697]
40. Nishikawa H, Qian F, Tsuji T, Ritter G, Old LJ, Gnjatic S, et al.Influence of $CD4^+CD25^+$ regulatory T cells on low/high-avidity $CD4^+$ T cells following peptide vaccination. J Immunol2006;176:6340–6. [PubMed: 16670346]
41. Mitsunaga M, Nakajima T, Sano K, Choyke PL, Kobayashi H. Near-infrared theranostic photoimmunotherapy (PIT): repeated exposure of light enhances the effect of immunoconjugate. Bioconjug Chem2012;23:604–9. [PubMed: 22369484]
42. Nagaya T, Sato K, Harada T, Nakamura Y, Choyke PL, Kobayashi H. Near Infrared Photoimmunotherapy Targeting EGFR Positive Triple Negative Breast Cancer: Optimizing the Conjugate-Light Regimen. PLoS One2015;10:e0136829.
43. Okuyama S, Nagaya T, Sato K, Ogata F, Maruoka Y, Choyke PL, et al.Interstitial near-infrared photoimmunotherapy: effective treatment areas and light doses needed for use with fiber optic diffusers. Oncotarget2018;9:11159–69. [PubMed: 29541404]
44. Maruoka Y, Nagaya T, Sato K, Ogata F, Okuyama S, Choyke PL, et al.Near Infrared Photoimmunotherapy with Combined Exposure of External and Interstitial Light Sources. Mol Pharm2018;15:3634–41. [PubMed: 29450993]
45. Mroz P, Hashmi JT, Huang YY, Lange N, Hamblin MR. Stimulation of anti-tumor immunity by photodynamic therapy. Expert Rev Clin Immunol. 2011;7:75–91. [PubMed: 21162652]
46. Sato K, Ando K, Okuyama S, Moriguchi S, Ogura T, Totoki S, et al.Photoinduced Ligand Release from a Silicon Phthalocyanine Dye Conjugated with Monoclonal Antibodies: A Mechanism of Cancer Cell Cytotoxicity after Near-Infrared Photoimmunotherapy. ACS central science. 2018; 4: 1559–69. [PubMed: 30555909]
47. Hoffman RM. Patient-derived orthotopic xenografts: better mimic of metastasis than subcutaneous xenografts. Nat Rev Cancer2015;15:451–2. [PubMed: 26422835]

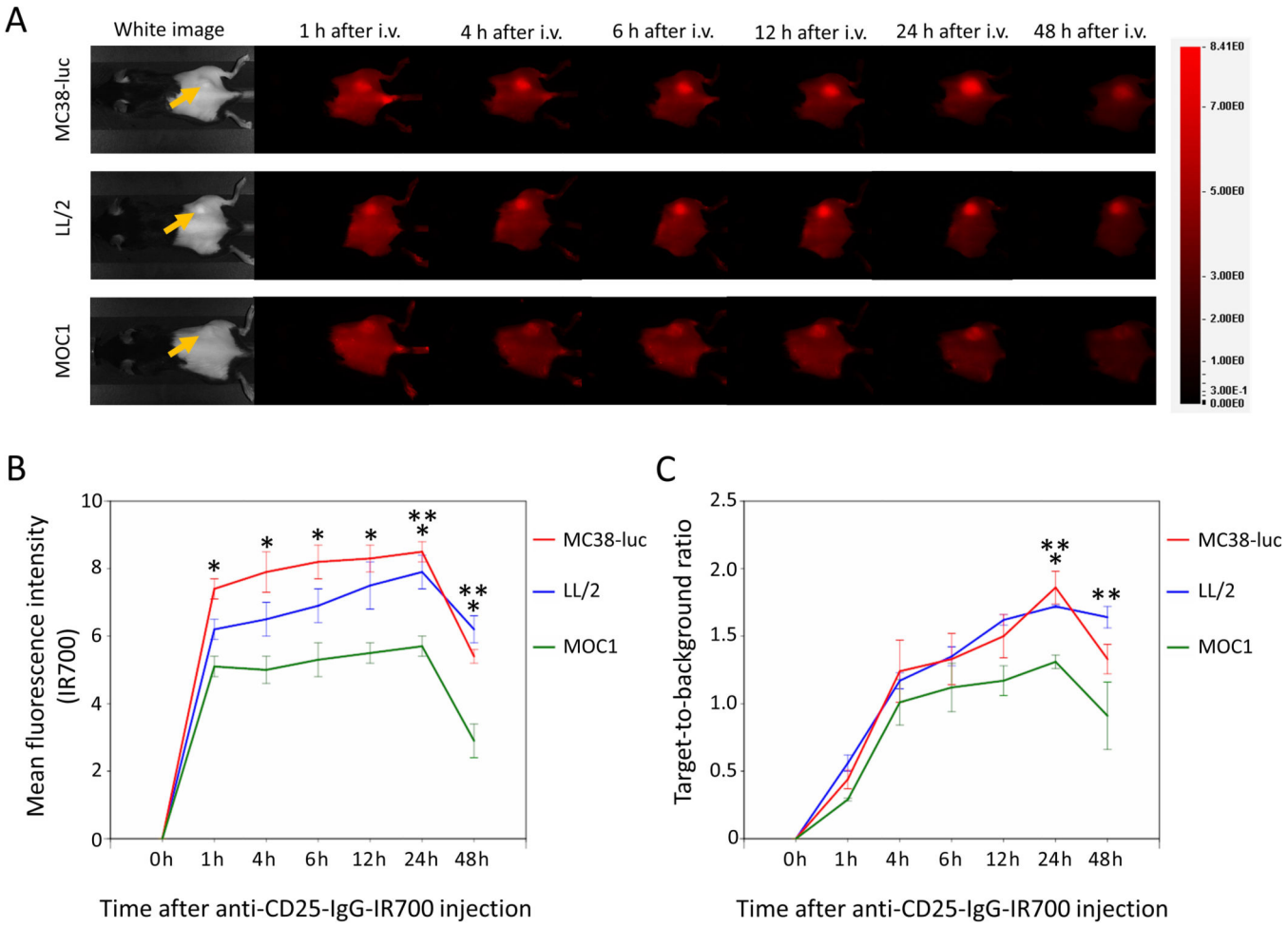

Figure 1. *In vivo* IR700 fluorescence imaging of MC38-luc, LL/2, and MOC1 tumors after injection of anti-CD25-IR700.

A. Real-time *In vivo* anti-CD25-IR700 fluorescence imaging of tumor-bearing mice at the indicated timepoints. The yellow arrows indicate the tumor locations. **B.** Quantitative analysis of mean fluorescence intensity in MC38-luc, LL/2, and MOC1 tumors (n=5/group, mean+/− SEM). *p<0.05, MC38-luc vs. MOC1 tumors, Tukey-Kramer test; **p<0.05, LL/2 vs. MOC1 tumors, Tukey-Kramer test. **C.** Quantitative analysis of target-to-background ratio in MC38-luc, LL/2, and MOC1 tumors (n=5/group, mean+/− SEM). *p<0.05, MC38-luc vs. MOC1 tumors, Tukey-Kramer test; **p<0.05, LL/2 vs. MOC1 tumors, Tukey-Kramer test.

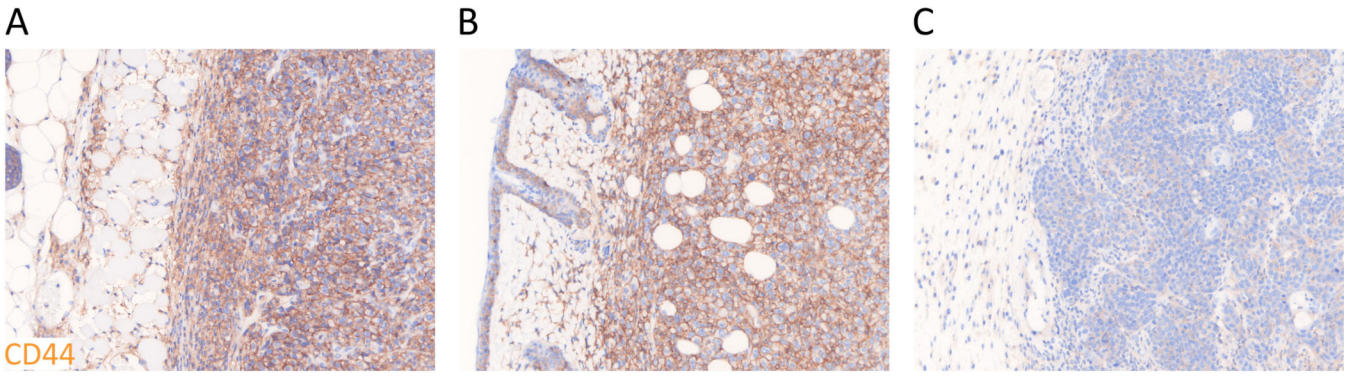

Figure 2. CD44 expression within MC38-luc, LL/2, and MOC1 tumors.

A-C. Immunohistochemistry staining was performed to examine CD44 expression as a target for NIR-PIT within (A) MC38-luc, (B) LL/2, and (C) MOC1 tumors without treatment. Representative images from at least three samples are shown (×200).

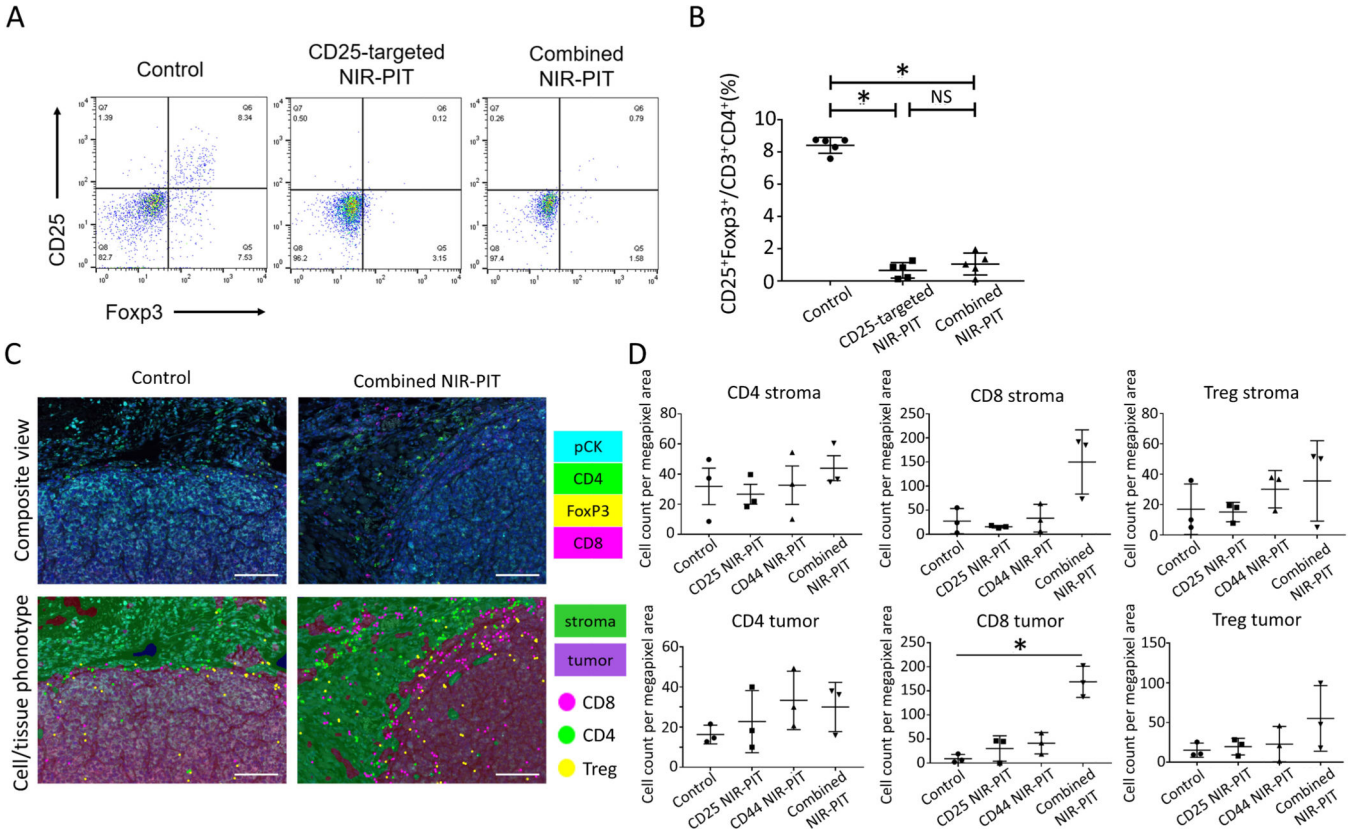

Figure 3. Immune correlative and functional effects of NIR-PIT in MC38-luc tumor-bearing mice.

A. Representative dot plots of live, $FOXP3^+CD25^+CD4^+$ T cells via flow cytometry in MC38-luc tumors (1 day after NIR light irradiation) treated with CD25-targeted NIR-PIT, combined CD44- and CD25-targeted NIR-PIT, and control tumors. **B.** Cell count ratios of $CD25^+FOXP3^+$ cells in $CD3^+$ $CD4^+$ cells within the tumors (n=5/group from single experiment, mean+/− SEM, *p<0.05, Tukey-Kramer test; NS: not significant. **C.** Representative multi-color immunofluorescence images (×200) for $CD8^+$ T cells, $CD4^+$ T cells, and Tregs infiltrating in TME of MC38-luc tumors (7 days after NIR light irradiation, n=3/group) treated with CD25-targeted NIR-PIT, CD44-targeted NIR-PIT, combined CD44- and CD25- targeted NIR-PIT (*right side*), and control tumors (*left side*). $CD8^+$ cells, $CD4^+FOXP3^-$ cells, and $CD4^+FOXP3^+$ cells were regarded as $CD8^+$ T cells, $CD4^+$ T cells, and Tregs, respectively. Scale bar represents 100um. **D.** Cell counts per megapixel in multi-color immunofluorescence images to quantitatively evaluate $CD4^+$ T cells, $CD8^+$ T cells, and Tregs infiltrating into the TME. (n=3/group from single experiment, mean+/− SEM, *p<0.05, t-test.

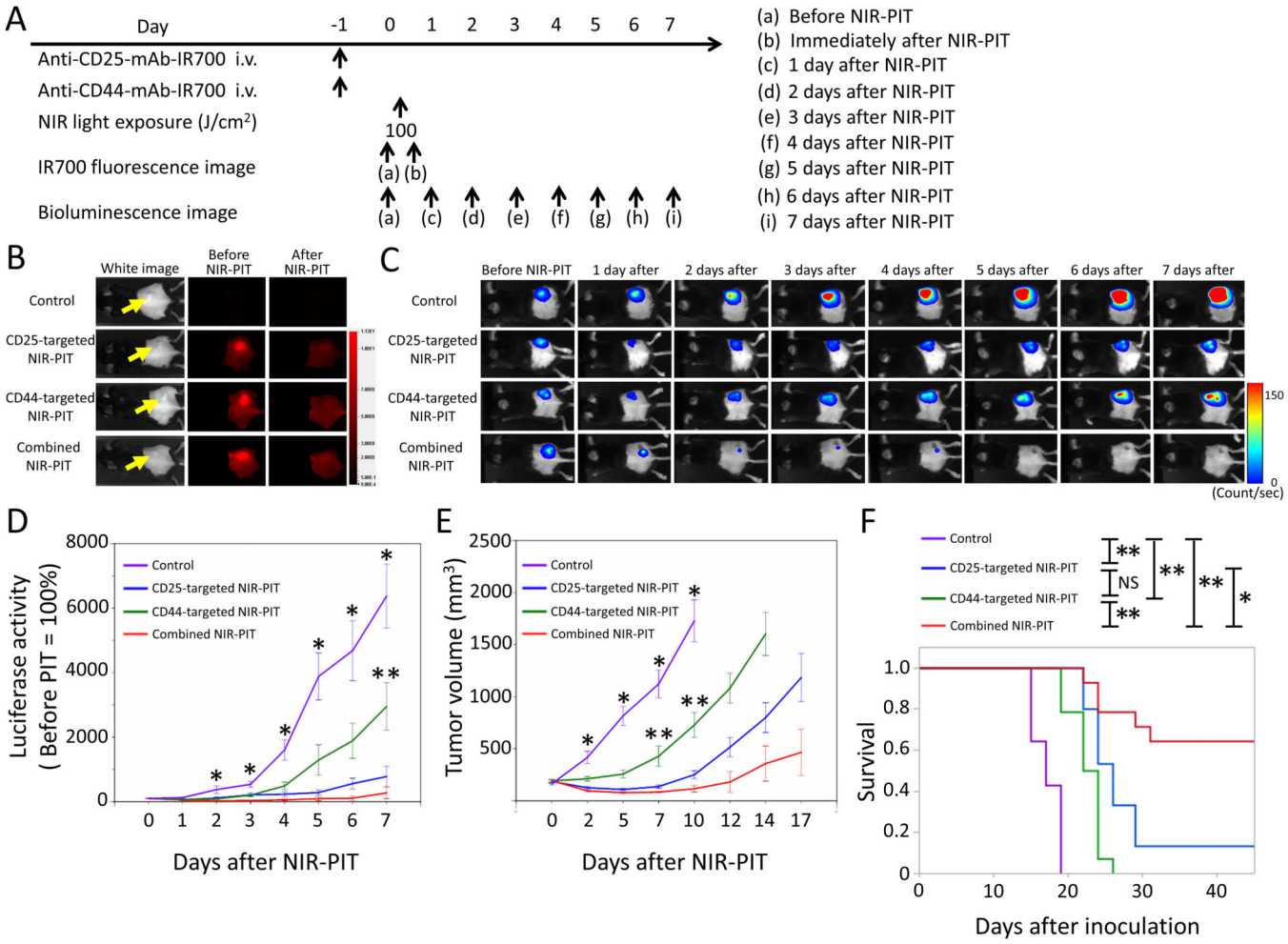

Figure 4. *In vivo* effect of CD25- and/or CD44-targeted NIR-PIT in MC38-luc tumors.

A. NIR-PIT regimen. Bioluminescence and fluorescence images were obtained at each time point as indicated. **B.** Real-time *in vivo* IR700 fluorescence imaging of tumor-bearing mice before and approximately 10 minutes after NIR-PIT. The yellow arrows indicate the tumor locations. **C.** *In vivo* bioluminescence imaging of tumor-bearing mice before and after NIR-PIT at the indicated timepoints. **D.** Quantitative analysis of luciferase activity before and after NIR-PIT in tumor-bearing mice. n≥10/group, mean+/− SEM, *p<0.05, control vs. the other groups, Tukey-Kramer test; **p<0.05, CD44-taregeted NIR-PIT vs. combined NIR-PIT group, Tukey-Kramer test. **E.** Tumor growth in control and all NIR-PIT–treated groups. n≥10/group, mean+/− SEM, *p<0.05, control vs. the other groups, Tukey-Kramer test; **p<0.05, CD44-targeted NIR-PIT vs. combined NIR-PIT group, Tukey-Kramer test. **F.** Survival curves for control and NIR-PIT–treated groups. n≥10/group, *p<0.05, **p<0.01, Log-rank test; NS: not significant.

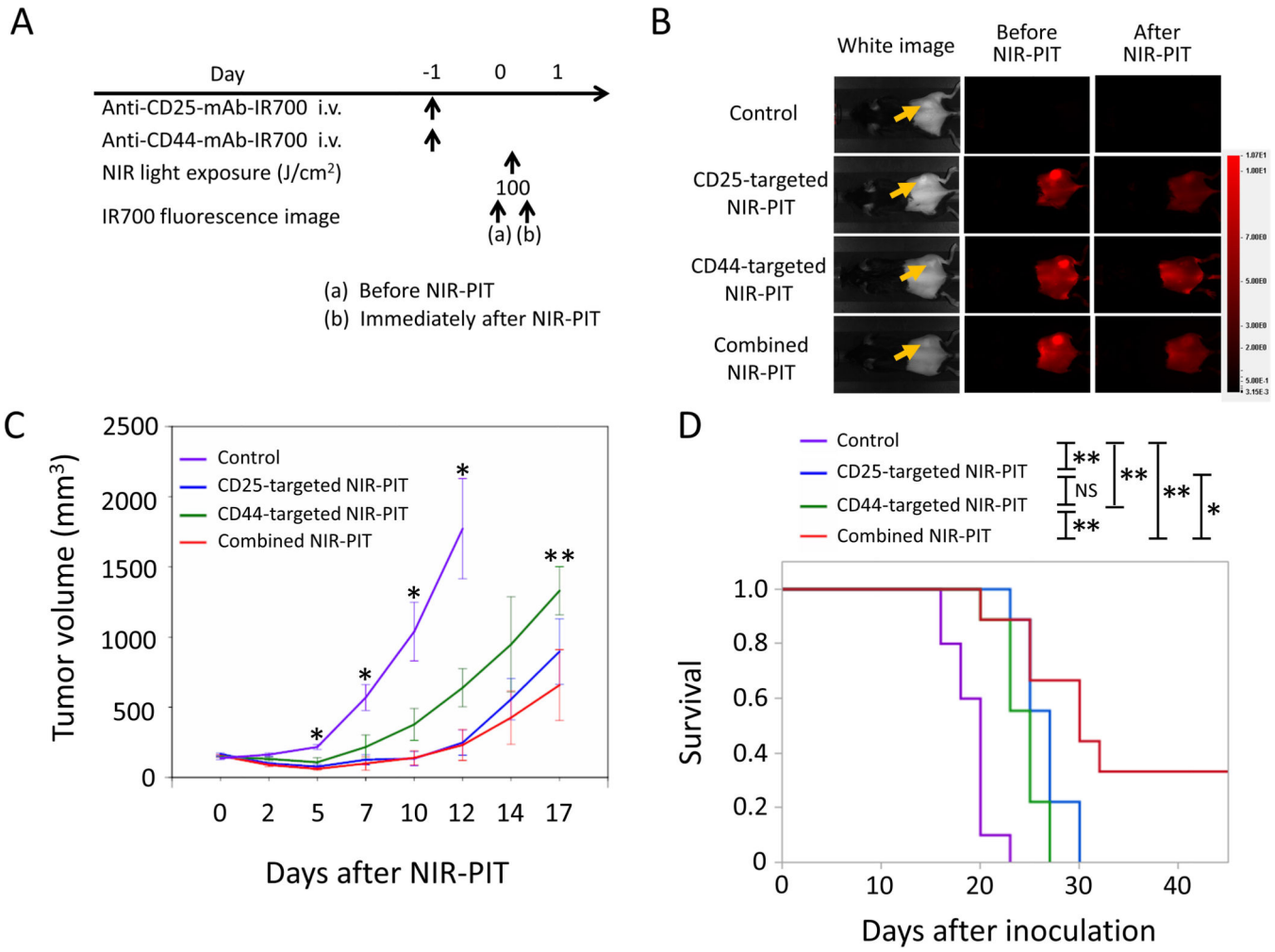

Figure 5. ***In vivo*** **effect of CD25- and/or CD44-targeted NIR-PIT in LL/2 tumors.**

A. NIR-PIT regimen. IR700 fluorescence images were obtained at each time point as indicated. **B.** Real-time *in vivo* IR700 fluorescence imaging of tumor-bearing mice before and approximately 10 minutes after NIR-PIT. The yellow arrows indicate the tumor locations. **C.** Tumor growth in control and all NIR-PIT–treated groups. n=9–10/group, mean+/− SEM, **p*<0.05, control vs. the other groups, Tukey-Kramer test; ***p*<0.05, CD44-targeted NIR-PIT vs. combined NIR-PIT group, Tukey-Kramer test. **D.** Survival curves for control and NIR-PIT–treated groups. n=9–10/group, **p*<0.05, ***p*<0.01, Log-rank test; NS: not significant.

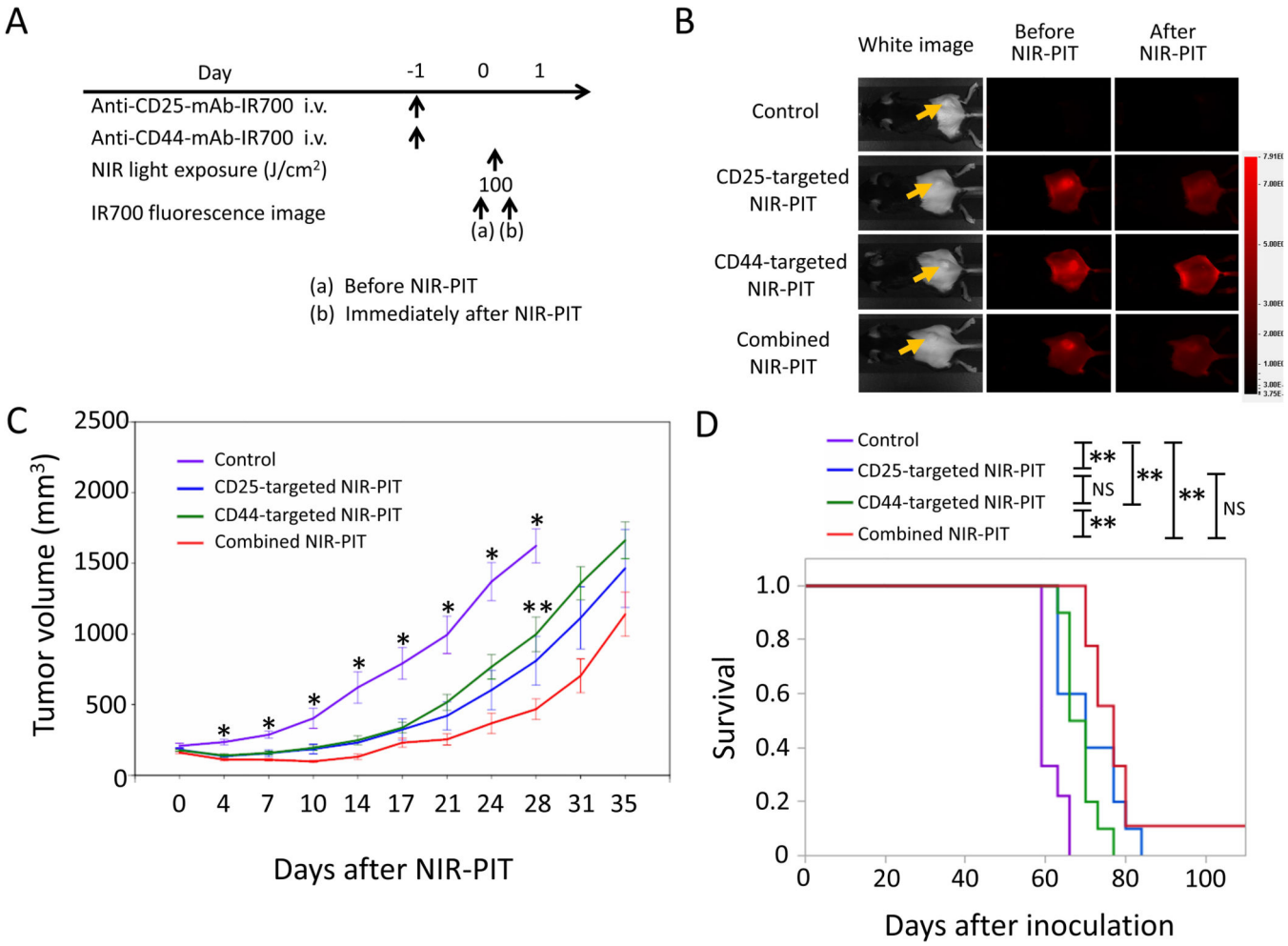

Figure 6. ***In vivo*** **effect of CD25- and/or CD44-targeted NIR-PIT in the MOC1 tumor model.** **A.** NIR-PIT regimen. IR700 fluorescence images were obtained at each time point as indicated. **B.** Real-time *in vivo* IR700 fluorescence imaging of tumor-bearing mice before and approximately 10 minutes after NIR-PIT. The yellow arrows indicate the tumor locations. **C.** Tumor growth in control and all NIR-PIT–treated groups. n=9–10/group, mean+/− SEM, *$p < 0.05$, control vs. the other groups, Tukey-Kramer test; **$p<0.05$, CD44-targeted NIR-PIT vs. combined NIR-PIT group, Tukey-Kramer test. **D.** Survival curves for control and NIR-PIT–treated groups. n=9–10/group, **$p<0.01$, Log-rank test; NS: not significant.

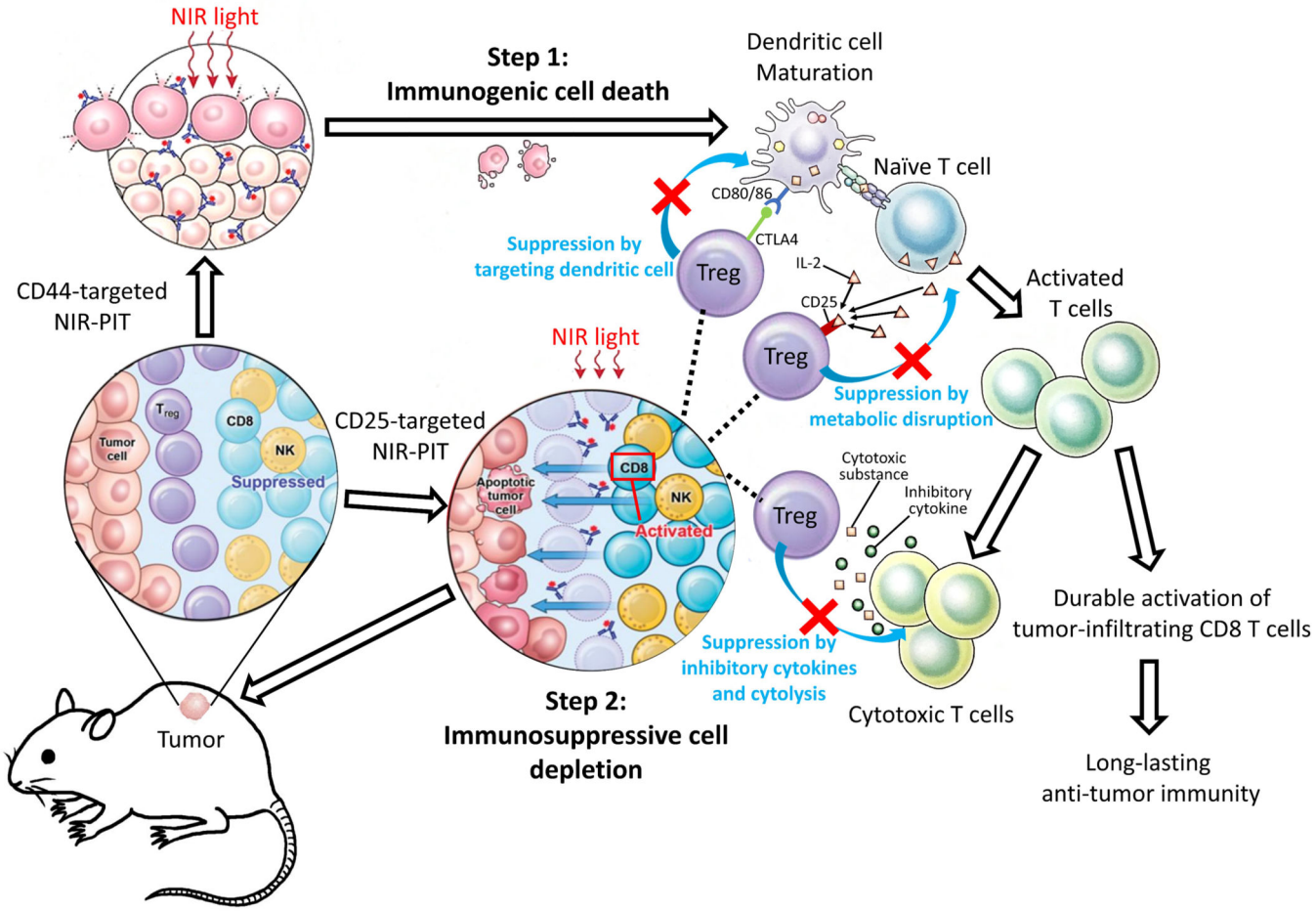

Figure 7. Proposed mechanism of combined CD44- and CD25-targeted NIR-PIT–induced immunotherapy.

$FOXP3^{+}CD25^{+}CD4^{+}$ Tregs limit antitumor immunity through suppression of effector T cells and NK cells by inhibitory cytokines and cytolysis, as well as by metabolic disruption with IL2 consumption and modulation of DC maturation or function. Combined CD44- and CD25-targeted NIR-PIT induces immunogenic cell death in $CD44^{+}$ tumors and selectively depletes Tregs with high CD25 expression. Step1: The process of immunogenic cell death caused by CD44-targeted NIR-PIT induces DC maturation. Step 2: Treg depletion induces activation and expansion of effector T cells and simultaneously, differentiation into tumor-specific T cells. Taken together, this combined NIR-PIT results in effective tumor killing and promotion of long-lasting antitumor immunity.